XXI Biannual Symposium on
Measuring Techniques in Turbomachinery
22-23 March 2012, Valencia, Spain

MeasTechSymp 2012

Characterization of a High Subsonic Wind Tunnel Test Section to Develop a Study Approach to Solve the Inverse Heat Conduction Problem

Ir. F. Baldani *, Ir. Dr. Prof. W. Bosschaerts *, Ing. R. Wagemakers *

* Royal Military School of Belgium
30 Avenue de la Renaissance, 1000 Brussels, Belgium
francesco.baldani@rma.ac.be

Abstract

Aim of the project is to propose a methodology to retrieve the heat flux through a finned heat exchanger placed downstream the fan of a turbine jet engine. The core of the Ph.D. study is the solution of the so called Inverse Heat Conduction Problem (IHCP). To solve the IHCP the surface temperature of the heat conducting body has to be used as boundary condition of the problem. The Infra Red thermography is used to measure the heat exchanger surface temperature. The experiments are performed at low speed and at high subsonic speed. These latter are performed in a blow-down wind tunnel capable to reach Mach numbers of the order of 0.75. The flow field in the blow-down wind tunnel test section is characterized exploiting the Constant Temperature Anemometry (C.T.A.) technique. To be able to perform multi-point measurements an 'ad-hoc' hot-wire probes support has been conceived and manufactured.

Keywords: Inverse Heat Conduction Problem, High Subsonic Speed, Infra Red Thermography, Constant Temperature Anemometry, hot-wire probes support

Introduction

The improvements in the manufacturing techniques as well as in the available materials push the aero-thermal engineers to find better solutions in order to improve engine performances. Indeed, improving turbine engine performances for military and civil purposes has a deep impact on thermal efficiency, fuel consumption, life-time and consequently on the achievement of the working standards required by the new laws in matter of environment such as noise and pollutant emissions.

Aim of the project is to study the heat transfer from a hot surface to a cold flow under conditions similar to those encountered by aircraft turbine engines, hence using the main flow of the engine to study a heat exchanger placed just downstream the fan. The main part of the research project deals with the solution of the "inverse heat conduction problem" which consists in imposing the object surface temperature as boundary condition and computing via numerical methods the resulting heat flux. The heat transfer coefficient is to be studied both locally and globally, since a global study of h is fundamental in the preliminary design phase while a local study of h is useful to understand the effects of the geometry on the local flow conditions (i.e. the turbulence intensity level) and on the achievable heat exchange.

We should remind that in a forced convection the flow is influenced by the amount of heat injected and that the flow rate versus the heat power injected is one of the major triggers for the flow that develops. On top of this the conduction within the plate adds up with the heat convection from the surface.

It should also be clear that to deepen the understanding of the heat transfer occurring in installations as finned heat exchangers one has always to consider that a simple superposition of the heat exchange phenomena is not enough. Indeed one should rather talk of "conjugate" heat transfer this latter being the actual coupled interaction of conduction and convection. For instance neglecting the effect of the wall conduction which greatly affects the temperature distribution will result in imposing unrealistic thermal boundary conditions at the solid-fluid interface leading to wrong heat transfer rates and coefficients.

For all these reasons the characterization of the wind tunnel test section flow field is a crucial issue. This is why the C.T.A. technique is chosen to characterize the flow field obtainable in the wind tunnel. The scheme in Figure 1 shows and summarizes the approach proposed to study the problem under analysis.

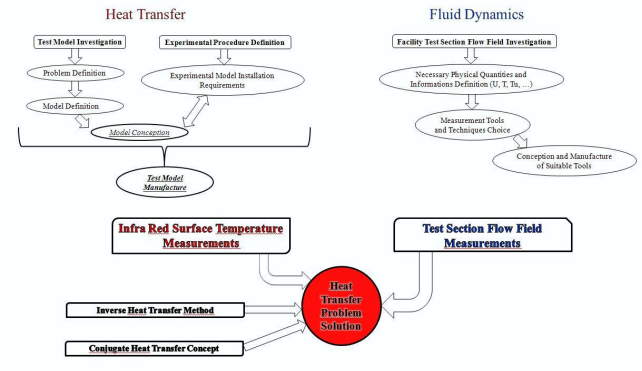

Figure 1 Proposed Study Approach

1 Conjugate Heat Transfer Concept

Since the studies conducted by Perelman[16] it is well known the importance of imposing correct boundary conditions when dealing with heat transfer problems involving a solid submerged in a flowing fluid. Indeed it is proven that in presence of large thermal gradient (in space) and if the fluid encounters obstacles (rib, fin, etc..) the thermal boundary conditions imposed (uniform T_{surf}, uniform heat flux) in the classical study (purely convective) are unrealistic. For this it is of crucial importance impose the correct boundary conditions at the solid-fluid interface. Therefore the conjugate heat transfer theory is the one to be used, being based on the concept that the effects of the solid domain conduction have to be coupled with the convection phenomenon happening over the solid surface. The idea is to perform surface temperature measurements of the finned heat exchanger under analysis with the I.R. thermography technique after having characterized the wind tunnel test section flow field exploiting the C.T.A. technique and/or the P.I.V. technique in order to be able to impose the correct boundary conditions for computing the surface heat flux distribution (via commercial FEM solvers or as proposed hereafter via a numerical solution of the so obtained Inverse Heat Conduction Problem)[10, 12, 15].

2 Transient Inverse Heat Conduction Problem

Determining local convection coefficients accurately or perform accurate local heat flux measurements is a hard and expensive task but for many cases the heat flux distribution is an indispensable parameter. For finned heat exchangers this task is particularly challenging [9, 11, 19]. Indeed heat transfer measurements at the fin base would introduce a thermal resistance between the primary surface and the fin due to the presence of the measurement device. Therefore the heat fluxes at the fin base have to be determined indirectly by measuring the heat fluxes through the extended surface and the primary surface. Among the available techniques to perform such measurements (heat flux sensors, local temperature measurements) the inverse heat conduction technique is probably the most suitable for our study. It is mainly used to estimate temperatures or heat fluxes at surfaces that are inaccessible for measurements. The advantage of this method is that the experimental studies can be performed under similar conditions and environment as during the operation. To solve an inverse heat conduction problem, a mathematical optimization method is required, which uses temperature measurements as input. Based on surface temperatures of a solid object, heat fluxes on one or more surfaces of the object can be estimated. So the need for internal temperature measurements can be omitted. Depending on the temperature measurement technique, the disturbance of the local temperature fields and heat flux distribution is limited or even absent. It also has the advantage that the temperature field in the whole object can be reconstructed based on surface temperature measurements, together with the coupled heat flux distribution. The proposed code allows the determination of the local convective heat exchange coefficient h(x,y,t), taking into account for the conductive flux in the heated plate. In general the heat flux can rise and fall abruptly and can be both positive and negative where negative values indicate heat losses from the surface. According to Beck, Blackwell and St.Clair [6] the source of heating is immaterial to the IHCP procedures. Mathematically the IHCP (for the 1-D case) can be described as in the set of equations 1 to 4.

$$\frac{\partial}{\partial x}\left(k\frac{\partial T}{\partial x}\right) = \rho c\frac{\partial T}{\partial t} \tag{1}$$

Where the thermal conductivity k, the density ρ and the specific heat c are postulated to be known functions of temperature.

$$T\left(x,0\right) = T_0\left(x\right) \tag{2}$$

$$\frac{\partial T}{\partial x} = 0\; at\; x = L \tag{3}$$

$$T\left(x_1,t_i\right) = Y_i \tag{4}$$

The objective is to estimate the surface heat flux at discrete times, t_i, from

$$q\left(t_i\right) = -k\left.\frac{\partial T\left(x,t_i\right)}{\partial x}\right|_{x=0} \tag{5}$$

After the paper by Beck, Blackwell and Haji-Sheikh [5] where can be found a review of some inverse heat conduction methods the method chosen to solve the IHCP is the so called 'function specification method' (FSM). The FSM has the advantage to be simple in concept and to not change the physics of the problem since the intrinsic parabolic nature of the problem is unchanged. The FSM is sequential in nature and thus computationally efficient and moreover the measurements in the distant future do not affect the 'present' estimates as for other methods [5]. The FSM can be used for linear and nonlinear problems and finite differences, finite elements or numerical convolution can be used. The method itself consists in minimizing, with respect to the heat flux q_M the sum of squares function as described by Eq. 6[5]. The equations 6 to 11 refer to measurements acquired by one sensor over multiple time steps.

$$S_M = \sum_{i=1}^{r} = \left(Y_{M+i-1} - T_{M+i-1}\right)^2 \tag{6}$$

which involves the times t_M, t_{M+1}, ..., t_{M+r-1}. Hence 'future' information is used to obtain q_M. Some

functional form for $q(t)$ for t_M to t_{M+r-1} is selected, the simplest being

$$q_{M+1} = q_M, \;\; i = 1, 2, \ldots, r \tag{7}$$

The calculated temperature T_{M+i-1} is expanded in a Taylor series for q_M obtaining

$$T_{M+i-1} = T_{M+i-1}|_{\hat{q}_M} + X_{M+i-1,M}\left(q_M - \hat{q}_M\right) \tag{8}$$

where $X_{M+i-1,M}$ is the sensitivity coefficient defined by

$$X_{M+i-1,M} = \frac{\partial T_{M+i-1,M}}{\partial q_M} \tag{9}$$

the resulting algorithm after minimizing Eq. 6 with respect to q_M is

$$\hat{q}_M = \hat{q}_{M-1} + \\ + \frac{\sum_{i=1}^{r}\left[Y_{M+i-1} - T_{M+i-1}|_{q_M = \cdots \simeq \hat{q}_M}\right] X_{M+i-1,M}}{\sum_{i=1}^{r} X_{M+i-1,M}^2} \tag{10}$$

Only $\hat{q}_M$ is retained for time t_M, and M is increased by one and the procedure is repeated. The iterative regularization method minimizes the whole domain function

$$S_M = \sum_{i=1}^{I} = (Y_i - T_i)^2 \tag{11}$$

where I is the total number of measurements. It should be noticed that in our analysis we use multiple sensors (i.e. surface temperature cartography $T(x, y, t)$ measured by the I.R. camera). Anyway this does not affect the exposed solution methodology but just the mathematical formalism.

2.1 IHCP Solution Validation

One can validate the proposed solution methodology for a flat plate of very thin thickness in a laminar flow. The validity of the proposed solution can be checked solving twice the direct model via a CFD software ($Fluent^{©}$ in our case). We compute first the heating phase with equations 17 to 22. In Eq. 17 the heat transfer coefficent h is computed from the Nusselt correlation (see equations 12 to 16).

$$Nu = 0.332 \cdot Re^{1/2} \cdot Pr^{1/3} \tag{12}$$

Equation 12 can be rewritten as follows to take into account for the Nusselt number evolution along the plate:

$$Nu(x) = \frac{0.332 \cdot Re(x)^{1/2} \cdot Pr^{1/3}}{\left[1 - \left(\frac{x_0}{x}\right)^{3/4}\right]^{1/3}} \tag{13}$$

If we take $x_0 = 0$ then the equation 13 reduces to:

$$Nu(x) = 0.332 \cdot Re(x)^{1/2} \cdot Pr^{1/3} \tag{14}$$

Since fluid properties (such as viscosity, diffusivity, etc.) can vary significantly with temperature, there can be some ambiguity as to which temperature one should use to select property values. The recommended approach is the use of the average of the wall and free-stream temperatures, defined as the film temperature $T_{film} = \frac{T_{surface} + T_{air}}{2}$.
Now recalling that the Nusselt number can be also expressed as reported in equation 15 we will be able, once $Nu(x)$ is known, to compute $h(x)$ as from equation 16.

$$Nu(x) = \frac{h(x) \cdot x}{k_{air}} \tag{15}$$

$$h(x) = \frac{Nu(x) \cdot k_{air}}{x} \tag{16}$$

The equation 12 holds for a laminar, isothermal, local situation with $Pr > 0.6$ which is the situation we will deal with imposing a flow velocity (U_∞) of 10 m/s and a flow bulk temperature (T_∞) of 18° C.

$$(dzdxdy)\,\lambda\left(\frac{\partial^2 T}{\partial x^2} + \frac{\partial^2 T}{\partial y^2}\right) + P\,(dzdxdy) \;\; = \\ \rho c_p \frac{\partial T}{\partial t}\,(dzdxdy) + hdxdy\,(T - T_\infty) \tag{17}$$

with as initial condition

$$T\,(x, y, 0) = T_0 \tag{18}$$

and as boundary conditions

$$-\lambda \left.\frac{\partial T}{\partial x}\right|_{x=0} = 0 \tag{19}$$

$$-\lambda \left.\frac{\partial T}{\partial x}\right|_{x=L} = 0 \tag{20}$$

$$-\lambda \left.\frac{\partial T}{\partial y}\right|_{y=0} = 0 \tag{21}$$

$$-\lambda \left.\frac{\partial T}{\partial y}\right|_{y=H} = 0 \tag{22}$$

The result of this first direct simulation is the surface 'hot' reference temperature cartography $T(x, y, t_1) = T_1$. The second direct simulation is performed to compute the cooling phase and therefore retrieve the surface 'cold' reference temperature cartography $T(x, y, t_2) = T_2$ (exploiting Eq. 23 and equations 18 to 22).

$$(dzdxdy)\,\lambda\left(\frac{\partial^2 T}{\partial x^2} + \frac{\partial^2 T}{\partial y^2}\right) = \rho c_p \frac{\partial T}{\partial t}(dzdxdy) + hdxdy\,(T - T_\infty) \tag{23}$$

It is now possible to use T_1 and T_2 as boundary conditions for the solution of the IHCP. The obtained result is reported in Figure 2.

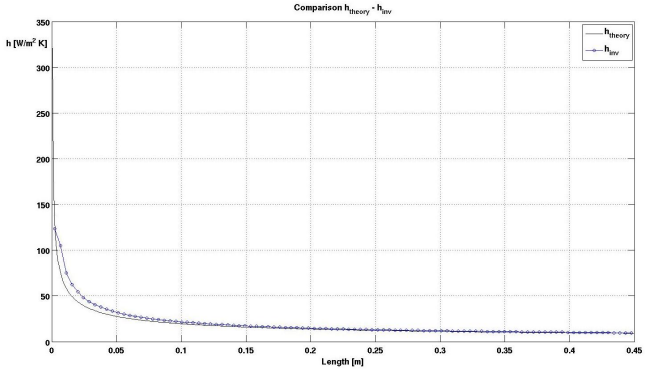

Figure 2 Theory - IHCP solution Comparison

3 Experimental Facilities and Set-up

The facility used for the high speed experiments is a blow-down wind tunnel where the air coming from a pressurized tank can be heated.
A velocity $U_{mean} \approx$ 30-230 *m/s* with a flow temperature $T_{mean} \approx$ 290-320 *K* are flow conditions that can be considered satisfying the similarity rules to those appearing at the inlet of an aircraft engine during various flight conditions. See Figure 3 for the working scheme of the installation. The test section sketch and the installation of the measuring tools are sketched in Figure 4.

The experimental set-up for the low speed experiments is pictured in Figure 5. In the picture it is possible to see the I.R. camera used to acquire the surface thermographs, a hot-wire rake used to check the test section velocity and the heating resistance together with its power supply.

4 Experimental Campaigns and Data Analysis

The following sections summarize the sets of experimental campaigns that have been conducted in order to characterize the high speed wind tunnel test section flow field and to validate the inverse heat conduction problem solution method.

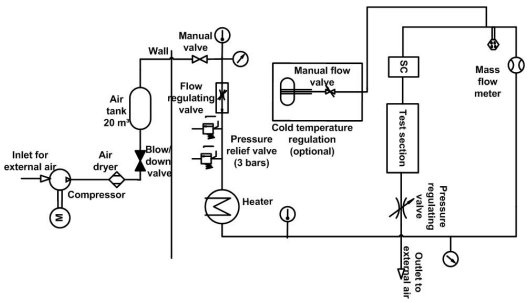

Figure 3 Facility Working Principle Diagram (Courtesy of ULB)

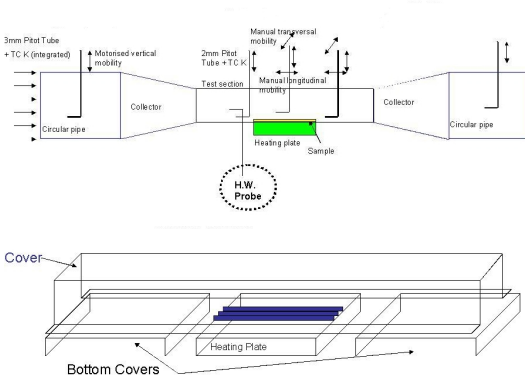

Figure 4 Test Section and Measuring Tools Installation Sketch (Courtesy of ULB)

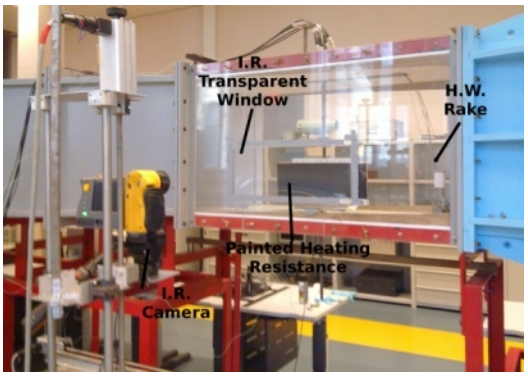

Figure 5 I.R. Low Speed Experiments Set-up

4.1 High Speed Experimental Campaign

Aim of the high speed experimental campaign is to characterize the blow-down wind tunnel flow field via the C.T.A. technique. Using hot-wire probes five different regimes of interest are investigated. A second experimental campaign is performed to measure the velocity profile and the effect of the presence of a finned heat exchanger in the section. A third series of experiments is performed to test the capabilities of a manufactured hot-wire probes rake.

4.1.1 Mean Flow Field Measurements

The test are performed with a plane bottom wall. The five investigated regimes classified according to the velocity and the mean total temperature of the fluid in the test sec-

tion are summarized in table 1.

Regime #	U_{mean}	T_{total}
1	230 m/s	315 K
2	160 m/s	305 K
3	130 m/s	300 K
4	60 m/s	295 K
5	30 m/s	295 K

Table 1 Tested Regimes

4.1.2 Traverses Experiments

This experimental campaign is performed with the finned heat exchanger placed in the test section but with no heat injection (i.e. no heat exchange between the finned surface and the flow) during the measurements. The experiments consist in hot-wire probe traverses in order to measure the velocity profiles before and after the prototype. The sketch in Figure 6 shows the positions and the locations where the experiments are performed.

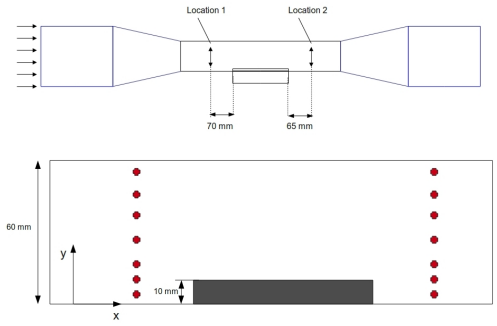

Figure 6 H-W. Traverses Experiments

According to the frame of reference shown in Figure 6 the positions analyzed for the two locations are: y = 6-11-16-26-36-46-56 *mm*. The measurements in the two locations are performed during two different experiments.

4.1.3 Hot-wire Rakes

A major issue while performing the traverses experiments is to keep perfectly constant the flow conditions in order to let the moving probe facing the same flow field. To overcome this problem a design for a hot-wire probes rake is proposed, so that the velocity could be measured in different positions at once. The designed support is based on a well known *NACA* 4 digits symmetrical wing. The manufactured 3 probes support installed in the test section can be seen in Figure 7.

The reasons why after some preliminary studies a symmetrical wing based on a NACA-0025 airfoil is chosen are reported next. The support has to be inserted in a high

Figure 7 Manufactured 3 Probes Support

velocity environment this means that big forces could occur. Therefore to greatly reduce the forces acting on the rake and consequently the need for stout holders any kind of shape creating important drag forces should be avoided. The area facing the flow should be as little as possible to reduce the blockage and consequently the interference with the free flow. Additionally when dealing with velocities of the order of 230 *m/s* reducing the vibrations of the support becomes also very important. The adopted solution besides satisfying the abovementioned requirements allows also to minimize the wake size drastically reducing the interference effects on other measuring tools installed behind the rake itself. After the validation of the 3 probes support we decided to manufacture a 5 probes support that could grant the vertical velocity profile measurement of the whole test section at once. The rake is pictured in Figure 8, the probes are installed at a distance of 12.5 *mm* from each other. In Figure 9 we can see the last version of the H.W. rake, prepared with molding plaster and where two thermocouples have been embedded in the support. This probe support has been tested only at low speed.

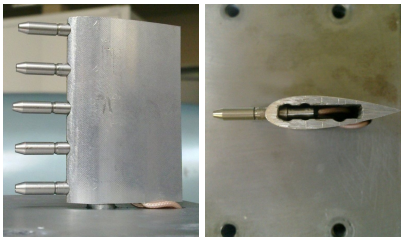

Figure 8 Manufactured 5 Probes Support

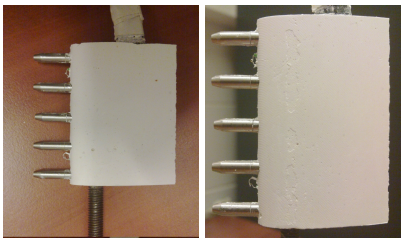

Figure 9 Manufactured 5 Probes Support (Plaster)

4.2 C.T.A. Data Analysis

When dealing with signals like those obtainable with the C.T.A. one can perform mainly three kind of analysis:

1. Descriptive static statistic analysis:
   - averaged values
   - skewness, kurtosis
   - variance, standard deviation
2. Spectral analysis
3. Signal correlation analysis
   - autocorrelation
   - cross-correlation

Since the C.T.A. technique is an indirect measurement technique a calibration law is required. Calibration units are available for this purpose, letting us associate to a known velocity the voltage measured by the hot-wire probe [18]. But this procedure cannot be exploited to analyze the data when the temperature varies during the measurements. Since the environment in which the hot–wire probe is placed is characterized by rather significant temperature variations, 6/7 *K* during the same regime and from 320 *K* to 295 *K* from the beginning to the end of a complete run, rather than a calibration curve a calibration surface with the temperature as additional variable would be required. The biggest issue to obtain such a calibration surface is that a dedicated wind tunnel is needed, where both the velocity and the flow temperature can be controlled. The one available at the Royal Military School can reach a maximum velocity of 30 *m/s* under controlled temperature conditions but during the experiments the velocity ranges between 40 *m/s* and 230 *m/s*. Therefore an alternative calibration procedure is needed. The "in-situ" calibration proposed consists in extracting the measured voltage, velocity and temperature for each investigated flow regime. The raw voltages are then corrected in temperature according to equation 25 and an iterative procedure implemented in $Matlab^{©}$ computes simultaneously the *"reference King's Law coefficients"*. The basic idea is to retrieve a "unique" calibration law that can be used even if the temperature is changing, the scheme in Figure 10 summarizes the strategy to obtain the proposed calibration curve.

In this way it is possible to perform experiments and exploit the acquired data to obtain a calibration law that is corrected in temperature. Equation 24 shows the King's Law while in equation 25 is reported the correction applied prior to linearize the data [14].

$$E_{corr}^2 = A_{ref} + B_{ref} \cdot U^{n_{ref}} \tag{24}$$

$$E_{corr} = E_{meas} \cdot \left(\frac{T_w - T_{ref}}{T_w - T_a} \right)^{0.5 \cdot (1 \pm m)} \tag{25}$$

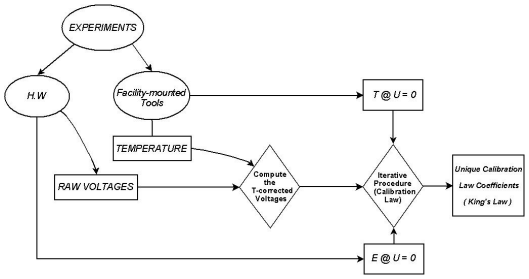

Figure 10 Unique Calibration Law Procedure Logical Scheme

where T_w is the wire temperature, T_{ref} is the reference temperature (in this case the temperature in the test section immediately before the experiment), T_a is the ambient temperature, measured by the facility mounted instrumentation. The parameter m is called *"Temperature Loading Factor"* and is suggested by Dantec for temperature correction purposes, it should be kept between 0.2 and 0.3 and added or subtracted depending on whether T_a is bigger or smaller than T_{ref} respectively. An example of the resulting "unique" calibration law is reported in Figure 11.

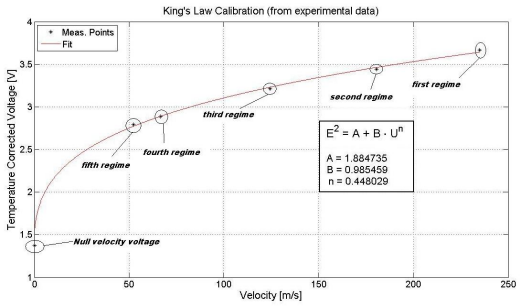

Figure 11 Unique Calibration Law Example

4.2.1 Correction for Fluid Temperature Drift

To obtain the actual velocities the reference King's law coefficients are "tuned" accordingly to the measured fluid temperature. The corrected King's law coefficients are computed as described by the set of equations 26.

$$\begin{cases} A_{corr} = \left(\dfrac{T_w - T_a}{T_w - T_0} \right)^{(1 \pm m)} \cdot \dfrac{K_{f_a}}{K_{f_0}} \cdot \left(\dfrac{Pr_{f_a}}{Pr_{f_0}} \right)^{0.2} \cdot A_{ref} \\ B_{corr} = \left(\dfrac{T_w - T_a}{T_w - T_0} \right)^{(1 \pm m)} \cdot \dfrac{K_{f_a}}{K_{f_0}} \cdot \left(\dfrac{Pr_{f_a}}{Pr_{f_0}} \right)^{0.33} \cdot \\ \qquad \cdot \left(\dfrac{\rho_{f_a}}{\rho_{f_0}} \right)^{n} \cdot \left(\dfrac{\mu_{f_a}}{\mu_{f_0}} \right)^{-n} B_{ref} \end{cases} \tag{26}$$

The air physical properties in equation 26 are computed at the temperatures T_{f_a} and T_{f_0} respectively the ambient and reference film temperatures obtainable as follows:

$$\begin{cases} T_{f_a} = \dfrac{T_w + T_a}{2} \\ T_{f_{ref}} = \dfrac{T_w + T_{ref}}{2} \end{cases} \tag{27}$$

So after the correction the King's calibration law should be rewritten as follows:

$$E^2 = A_{corr} + B_{corr} \cdot U^n \tag{28}$$

Eventually the velocity in the wind tunnel test section is computed as reported by the expression in equation 29.

$$U = \left(\frac{E^2 - A_{corr}}{B_{corr}} \right)^{\frac{1}{n}} \tag{29}$$

4.3 Low Speed Experimental Campaign: I.R. Analysis

Aim of the low speed experimental campaign is to validate the methodology and the tools to be used to solve the IHCP In a low speed wind tunnel a quasi-2D heating resistance has been placed in the test section and surface thermographs are recorded ([8]) in order to exploit a numerical procedure capable to compute the heat conduction coefficient. The analysis of the requirements and of the constraints led to the conception of the experimental model as sketched in Figure 12.

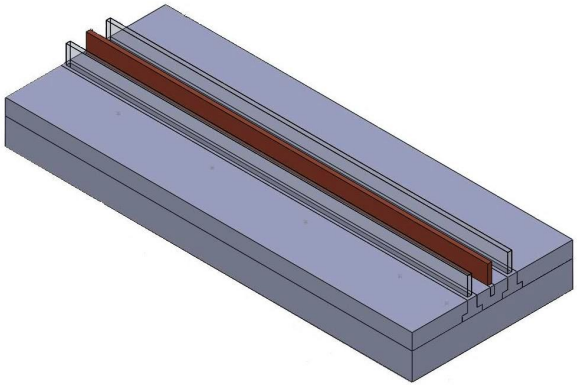

Figure 12 Experimental Model Conception Sketch

The real heat exchanger is reproduced by means of a central fin, made of copper and acting as heating resistance. On the two sides of this central fin is placed a set of two fins made of I.R. transparent material (CaF_2 for instance). The idea is to exploit the prototype symmetry in order to simplify its testing model. Additionally using a heating resistance as central fin allows us to know and control the heat injected.
According to the mentioned needs the proposed procedure to perform the experiments can be summarized as follows:

1. Heat the central fin up to the maximum allowed temperature
2. Open the facility valve in order to reach a stabilized velocity
3. Increase the heating power injected in the fin accordingly to the velocity increase in order to keep the heating resistance at a constant temperature
4. Once the velocity and the fin T_{surf} are stabilized acquire a reference surface thermograph (hot surface)
5. Switch off the heating resistance
6. Record the fin T_{surf} evolution with the I.R. camera (cold surface)
7. Solve the IHCP via the numerical calculation

For what concerns the experiments presented in this work one should remind that the configuration proposed in Figure 12 has been replaced by a stand alone very thin ($0.25\,mm$) but with a bigger surface ($170\,x\,450\,mm$) heating resistance for a sake of simplicity. The heating resistance is of the order of 20Ω and it is fed with $12 Volts$. The flow velocity in the wind tunnel test section is $10\,m/s$. The above mentioned procedure is then applied as described.

4.4 I.R. Experiments Data Analysis

The code exploited to solve the IHCP needs to be fed with a matrix of data representing the thermograph acquired by the I.R. camera. Therefore once recorded, the images must be prepared in order to be used as boundary conditions for the numerical method proposed. The rebuilding procedure could be summarized as follows:

1. An I.R. image where the color map palette is present is needed in order to be able to know the color levels to be linked to the temperature levels (see Figure 13).
2. Retrieve a vector able to translate the R(ed)-G(reen)-B(lue) data contained in the I.R. images into a matrix containing the surface temperature.
3. Pick up conveniently a frame from the recorded I.R. video, this will be the cold surface and fix the time step for the numerical solution (see Figure 14).
4. Translate the image into a $Matlab^{©}$ exploitable matrix.
5. Crop the image in order to contain only the surface of interest (i.e. only the flat plate and not the supports, etc. ...), see Figure 15.

Once prepared the I.R. images for the analysis one should just insert the right surface dimensions, time step and material characteristics in the script and feed the script with the hot surface and the cold surface informations matrices [4].

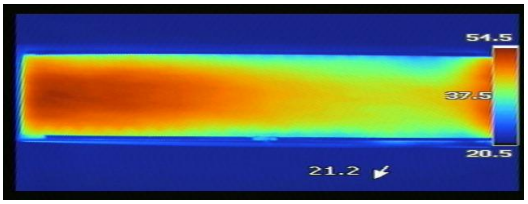

Figure 13 Color Vs. Temperature Levels

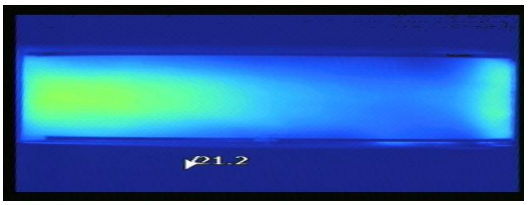

Figure 14 Cold Surface I.R. Image

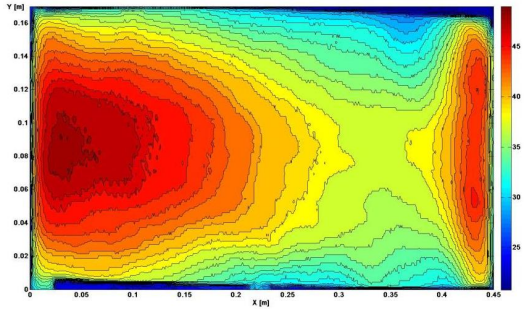

Figure 15 Cropped and Translated Image Example

5 CFD Low Speed Simulation

The purpose of these simulations is to check the behavior of the hot-wire probes support when inserted in the flow field. For this work the calculations have been used also to define the distance at which should be placed the heating resistance used for the I.R. experimental campaign. Indeed it is important to reduce at the maximum the influence of the wake released by the probe rake so that the recorded I.R. images depict the actual situation of a "hot" object submerged by an undisturbed "cold" flow. In Figure 16 is reported the geometry used to perform the simulations, it is possible to notice that the probe prongs and the wires are not modeled.

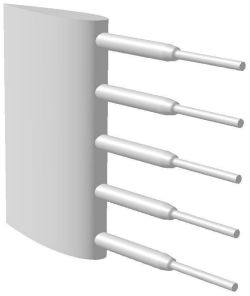

Figure 16 H.W. Rake Model

The model is created with the open source software K-3D ($http : //www.k-3d.org/$) while the mesh is produced with the automatic mesher $HEXPRESS^{TM}/Hybrid$. The calculations have been performed with the commercial solver $Fluent^{©}$. The domain reproducing the R.M.A. wind tunnel test section ($60\ cm\ x\ 60\ cm\ x\ 120\ cm$) is of about two millions cells. The 3-D steady state simulations have been performed using a standard $k-\epsilon$ turbulence model and the $Fluent^{©}$ enhanced wall treatment option enabled. The discretization schemes used are the $Fluent^{©}$ standard scheme for the pressure and the first order upwind scheme for the momentum, the turbulent kinetic energy and the turbulent dissipation rate. The velocity used for the simulation is the same as the one used for the I.R. test, $10\ m/s$.

6 Results

In this section are presented the obtained results. The flow field analysis of the blow-down wind tunnel are presented first. The low speed I.R. analysis experiment are only partially presented as they are performed for validation purposes and the whole methodology could not be fully discussed in this article. Eventually are presented the numerical simulations of the H.W. rake behavior performed at low speed.

6.1 Mean Flow Field Results

It is of crucial importance to characterize the turbulence in the testing chamber, the size of the turbulent scales and the frequency content. In Table 2 are summarized the results of the static statistic analysis and of the autocorrelation analysis for each flow regime [1, 2, 7, 13, 17].

Table 2 Experimental Campaign Results

Regime	*1*	*2*	*3*	*4*	*5*
$U_{meas}\ [m/s]$ (Pitot)	226.29	180.65	126.35	72.33	45.33
$U_{comp}\ [m/s]$ (H.W.)	234.19	170.57	123.10	71.04	47.26
Uncertainty $[m/s]$	± 4.47	± 4.44	± 4.08	± 0.99	± 0.35
Uncertainty %	1.91	2.60	3.32	1.39	0.74
Re_d	42.25	31.25	22.81	13.31	8.91
$Mach$ number	0.66	0.49	0.35	0.21	0.14
$T_{mean}\ [K]$	≈ 315	≈ 307	≈ 301	≈ 296	≈ 293
R.M.S.	5.615	3.398	2.846	1.753	1.267
Variance	31.523	11.549	8.098	3.072	1.604
Turbulence Intensity %	2.397	1.992	2.312	2.467	2.680
Skewness	-0.695	-0.506	-0.320	-0.314	-0.286
Kurtosis	3.655	3.791	3.483	3.565	3.512
Int. Length Scale $[mm]$	37.897	38.572	41.617	20.740	19.330
Taylor Micro Scale $\lambda\ [mm]$	6.795	4.855	4.163	2.739	2.468
Dissipation Rate $\epsilon\ [m^2/s^3]$	283.83	200.56	189.11	163.86	104.82
Kolmogorov Length Scale $\eta\ [mm]$	0.0931	0.1003	0.1010	0.1038	0.1155

The frequency analysis is performed exploiting the F.F.T. (Fast Fourier Transform) algorithm of Matlab which uses a special version of the discrete Fourier transform to filter the data. The error analysis for the presented results is performed according to the error propagation theory (the Kline-McClintock approach) always using a confidence interval of the 95%.

6.2 Hot-wire Traverses Results

The measures, coupled with pressure measurements, allow computing the pressure losses caused by the presence of the heat exchange. The test conditions repeatability being

one of the main issues the results presented cannot be retained quantitatively precise. Especially since the traverses at the two locations have been performed during two different test. However the experimental campaign gives meaningful information about the general flow field behavior [3].

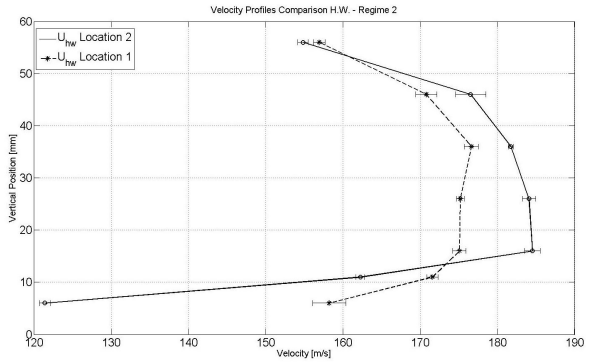

Figure 17 Velocity Profiles - H.W. Measures

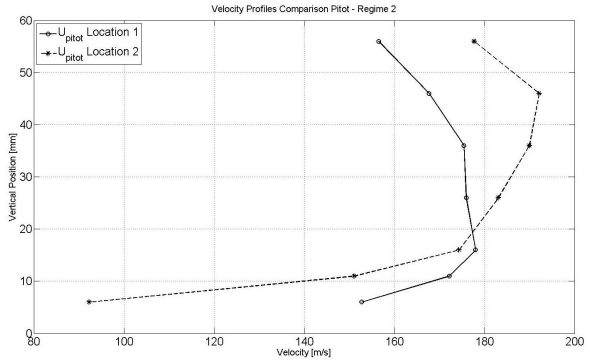

Figure 18 Velocity Profiles - Pitot Measures

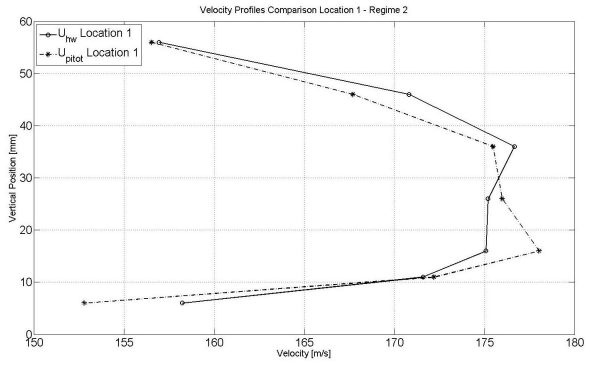

Figure 19 Velocity Profiles - Location 1, H.W. - Pitot Comparison

From Figure 19 and Figure 20 we can notice a discrepancy between the measurements performed with the hot-wire and the Pitot tube that seems to be mainly due to the fact that the wind tunnel is a blow-down facility. In facts with such facilities one of the biggest issues is to be certain to have exactly the same flow conditions for enough time

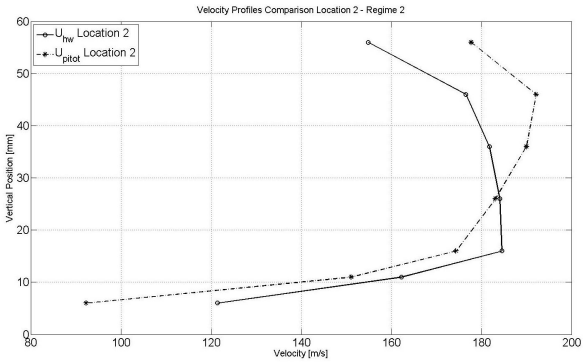

Figure 20 Velocity Profiles - Location 2, H.W. - Pitot Comparison

to perform a full traverse analysis. If we compare these results with the results in table 3 it is clear as performing multi-point measurements gives much more reliable measurements since we are certain that the flow conditions will be the same.

6.3 Hot-wire Rake Results

Since the wind tunnel is exploited in parallel by ULB and some modifications have been performed on it the results obtained with the hot-wire rakes should not be compared with above reported results. The main purpose of the performed experiments is to validate the manufactured rakes.

Regime	***Position***	U_{meas} Pitot	U_{meas} H.W.
1	1	$\approx 205.04\ m/s$	$\approx 205.64\ m/s$
	2	$\approx 207.01\ m/s$	$\approx 207.95\ m/s$
	3	$\approx 201.64\ m/s$	$\approx 203.40\ m/s$
2	1	$\approx 177.59\ m/s$	$\approx 171.01\ m/s$
	2	$\approx 173.34\ m/s$	$\approx 173.70\ m/s$
	3	$\approx 169.77\ m/s$	$\approx 170.78\ m/s$
3	1	$\approx 120.89\ m/s$	$\approx 121.88\ m/s$
	2	$\approx 124.40\ m/s$	$\approx 125.97\ m/s$
	3	$\approx 119.61\ m/s$	$\approx 124.54\ m/s$

Table 3 H.W. Rake 3 Probes Vs. Pitot

In table 3 are reported the velocities measured with the 3-probes support and a Pitot tube at the same positions but at a different distance from the test section inlet during the same test. It is easy to understand as the possibility to simultaneously measure the whole velocity profile drastically reduce the uncertainty linked to the capacity of maintaining exactly the same flow conditions for a long period of time. Therefore the accuracy of the velocity profiles measured with the rake is much higher and the profile shape gives indications on the actual test section flow field being not linked to the wind tunnel working parameters controlled by the operator.

6.4 CFD Simulation Results

In Figure 21 is plotted the computed velocity profile along the x-axis extracted from the wing trailing edge to the end of the numerical domain.

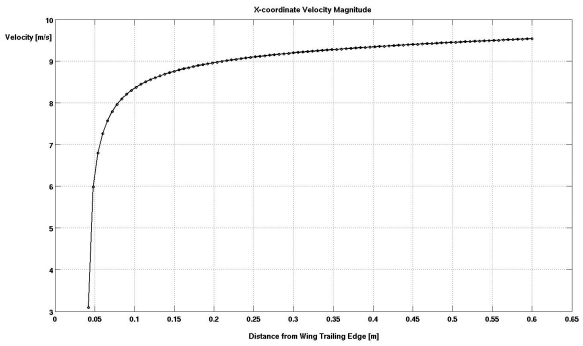

Figure 21 X-coordinate Velocity Plot

It is possible to notice that after 35 cm the influence of the rake wake starts being negligible, this why the heating resistance used for the I.R. experiment has been placed at about 40 cm from the probe support.

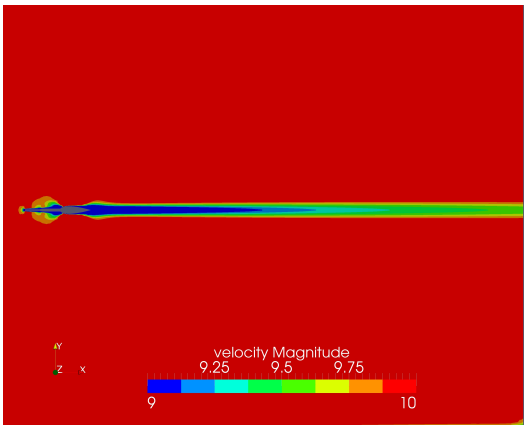

Figure 22 CFD-computed Velocity Contour Plot

From the contour plot reported in Figure 22 it is possible to see the influence of the presence of the rake in the whole domain. The results obtained could be used for comparison with oil flow visualization. This will be more interesting when moving to the high velocity case as the oil visualization allows to clearly see if the transition to supersonic occurs and where the flow in case detach from the wing surface.

6.5 IHCP Solution Results

Hereafter, in Figure 23, we can see a cartography of the convective heat transfer coefficient obtained exploiting the numerical solution of the IHCP. The results refer to the experiments performed with a time step of 5 seconds between two I.R. images and the flow is coming from the right side. The reason why the highest value of h is not located where the flow first impact the heated plate is due to the fact that the plate itself is installed on thick support in order to respect the boundary conditions (see equations 19 to 22) required by the IHCP solution. One should also notice that a regularization method is applied for the results presented.

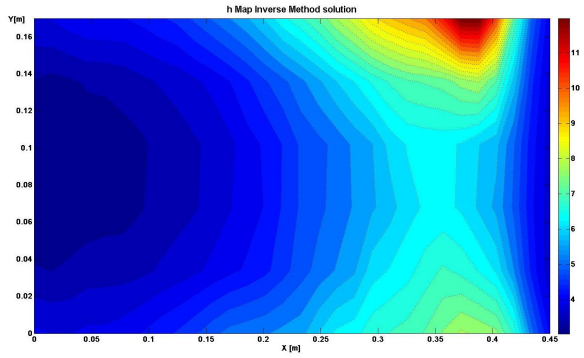

Figure 23 $\mathbf{h_{surf}}$ Cartography

Figure 24 $\mathbf{h_{surf}}$ Plot at the Plate Center Line

7 Conclusions

The analysis performed to check the flow field quality makes us assume that modifications should be performed on the wind tunnel. Indeed the very low turbulence level, together with the almost parabolic velocity profiles measured, let us assume that flow could probably not be fully developed when entering the test section. Though the absence of spectral peaks lets us deduce that the turbulence in the flow field is homogeneous and no frequency correlated structures are present (no vortex shedding or other phenomena). This leading to the conviction that performing minor modifications should be enough to improve the flow field quality. The coupling of Pitot tube and hot-wire probe traverse measurements shows that the general behavior of the flow field is maintained almost constant. Nevertheless it also testifies that the wind tunnel is not able to reproduce exactly the same conditions (p_{tot} profile, U profile, etc..) for two consecutive tests. The test performed with the hot-wire probes rake show the goodness of the support chosen design in order to overcome the main issue affecting a blow-down facility: maintain exactly the same working conditions for a long period of time. Indeed the rake allowed us to measure the velocity at five different positions instantaneously without affecting significantly the

flow field itself. The obtained results have been taken into account by the U.L.B. engineers while conceiving a revised version of the facility that is now under construction. The flow field of this new wind tunnel will be investigated in the next months.

For what concerns the numerical solution of the IHCP the validation test performed gave encouraging results. The lesson learned from the preliminary test performed is that one has to carefully prepare the experimental set-up in order to reduce as much as possible the heat losses (very high thermal insulation on the sides and on the back face of the fin). Furthermore prepare the experimental set-up to work with a finned heat exchanger at high subsonic velocity will be even more challenging. Nevertheless the task to validate the methodology and develop a consistent approach to this kind of analysis can be considered as accomplished. The simulations performed over the H.W. probe rake have been very helpful to correctly prepare the I.R. low velocity experimental set-up. Additionally the geometry and the meshing procedure are now well established so that it will be easier to move to the high subsonic velocity case.

8 Future Developments

One of the main and more imminent task will be to check the flow field quality in the revised version of the blow-down wind tunnel. Besides this task the capabilities of the H.W. rake made in plaster should be validate, indeed CFD simulations and flow oil visualization at high speed are scheduled in order to accomplish the task. The set-up for the I.R. experiments should be modified in order to let a flat velocity profile reach the heated plated. An enhanced regularization parameter based on the variation of the heat flux gradient is under validation and should be included in the proposed algorithm to solve the IHCP. Additionally the whole procedure should be optimized for a flow reaching $M \approx 0.7$ where possible issues could be the very small amount of time to grab I.R. images, the flow stabilization and the fin temperature stabilization.

Acknowledgments

I would like to thankfully acknowledge the "TEMPO Laboratory" of the University of Valenciennes guided by Professor Souad Harmand for giving me the opportunity to exploit their knowledge on the IHCP.

I also would like to sincerely thank the ULB research engineer Nicolas Heintz for the months of work performed together and the availability he showed.

References

[1] AIAA. *Preliminary Measurements of Velocity, Density and Total Temperature Fluctuations in Compressible Subsonic Flow*, Reno, NV, January 1983. AIAA.

[2] AIAA. *Turbulence in Complex Flows: A Selected Review*, Reno, NV, January 1992. AIAA.

[3] F. Baldani and W. Bosschaerts. Turbulence measurements in a high subsonic non-isothermal flow field. turbine engines inlet conditions analysis. *Conference Proceedings*, (ISABE-2011-1815), Gothenburg - September 2011.

[4] F. Baldani, W. Bosschaerts, and R. Wagemakers. High velocities wind tunnel flow field investigation and heat exchanger infra-red analysis. part 1: Experimental set-up, experiments and first results. *Conference Proceedings*, (ISAIF10-11), Brussels - July 2011.

[5] J. Beck, B. Blackwell, and A. Hoji-Sheikh. Comparison of some inverse heat conduction methods using experimental data. *International Journal of Heat Mass Transfer*, (Vol. 39, pp. 3649-3657), 1996.

[6] J. Beck, B. Blackwell, and C. S. C. Jr. *INVERSE HEAT CONDUCTION - Ill-posed Problems*. International Text Books in Mechanical Engineering. Wiley Interscience Publication, first edition edition, 1985.

[7] H. Bruun. *Hot–wire Anemometry, Principles and Signal Processing*. Oxford University Press Inc., 1995.

[8] G. Cardone, T. Astarita, and G. Carlomagno. Wall heat transfer in static and rotating 180 degrees turn channels by quantitative infrared thermography. *Re. Gén. Therm.*, (37, 644-652), 1998.

[9] F. Coletti. *Coupled Flow Field and Heat Transfer in an Advanced Internal Cooling Scheme*. PhD thesis, 2010.

[10] F. Coletti, A. Armellini, T. Arts, and C. Scholtes. Aero-thermal investigation of a rib-roughened trailing edge channel with crossing jets - part ii: Heat transfer analysis. *ASME paper No. GT2008 - 50695*, 2008.

[11] B. Cukurel, T. Arts, and C. Selcan. Conjugate heat transfer characterization in a ribbed cooling channel. *Conference Proceedings*, (ISAIF10-161), Brussels - July 2011.

[12] P. H. Groeber and D. S. Erk. *Fundamentals of Heat Transfer*. McGraw-Hill Series in Mechanical Engineering. McGraw-Hill Book Company, INC., third revised edition by dr. u. grigull edition, 1962.

[13] D. Hanson and K. Horan. Turbulence/cascade inter-

action: spectra of inflow, cascade response and noise. (A98-30871), 1998.

[14] F. E. Jorgensen. *How to measure turbulence with hot–wire anemometers*. Dantec Dynamics, Tonsbakke 16-18, DK-2740 Skovlunde, Denmark, 2005.

[15] F. Kreith. *Principles of Heat Transfer*. International Text Books in Mechanical Engineering. International Textbook Company Ltd, 158 Buckingham Palace Road London, second revised edition edition, 1965.

[16] T. Perelman. On conjugated problems of heat transfer. *International Journal of Heat Mass Transfer*, (Vol. 3, pp. 293-303), 1961.

[17] P. Stainback and K. Nagabushana. Review of hot-wire anemometry techniques and the range of their applicability for various flows. *Electronic Journal of Fluids Engineering, Transactions of the ASME*.

[18] Various. *Measurement Techniques in Fluid Dynamics - An Introduction*. VKI Lecture Series. von Karman Institute, second revised edition edition, 2001.

[19] A. Willockx. *Using the Inverse Heat Conduction Problem and Thermography for the Determination of Local Heat Transfer Coefficients and Fin Effectiveness for Longitudinal Fins*. PhD thesis, 2009.